


Mapping predicted biomass in cereal rye using 3D imaging and geostatistics

April M. Dobbs¹, Avi S. Goldsmith¹, Daniel Ginn², Søren Kelstrup Skovsen³, Muthukumar V. Bagavathiannan⁴, Steven B. Mirsky⁵, Chris S. Reberg-Horton⁶ and Ramon G. Leon⁷ 

Research Article

Cite this article: Dobbs AM, Goldsmith AS, Ginn D, Skovsen SK, Bagavathiannan MV, Mirsky SB, Reberg-Horton CS, Leon RG (2024). Mapping predicted biomass in cereal rye using 3D imaging and geostatistics. *Weed Sci.* doi: [10.1017/wsc.2024.62](https://doi.org/10.1017/wsc.2024.62)

Received: 16 January 2024

Revised: 6 June 2024

Accepted: 16 July 2024

Associate Editor:

Debalin Sarangi, University of Minnesota

Keywords:

Cover crop; point cloud; structure-from-motion; weed suppression

Corresponding author:

Ramon G. Leon; Email: rleon@ncsu.edu

¹Graduate Research Assistant, Department of Crop and Soil Sciences, North Carolina State University, Raleigh, NC, USA; ²Postdoctoral Research Associate, Department of Soil and Crop Sciences, Texas A&M University, College Station, TX, USA; ³Postdoctoral Research Associate, Department of Electrical and Computer Engineering, Aarhus University, Aarhus, Denmark; ⁴Billie Turner Professor of Production Agronomy, Department of Soil and Crop Sciences, Texas A&M University, College Station, TX, USA; ⁵Research Ecologist, Sustainable Agricultural Systems Lab, USDA-ARS, Beltsville, MD, USA; ⁶Blue Cross and Blue Shield of North Carolina Foundation/W.K. Kellogg Distinguished Professor, Department of Crop and Soil Sciences, North Carolina State University, Raleigh, NC, USA and ⁷William Neal Reynolds Distinguished Professor and University Faculty Scholar, Department of Crop and Soil Sciences, North Carolina State University, Raleigh, NC, USA

Abstract

Cover crops are becoming an increasingly important tool for weed suppression. Biomass production in cover crops is one of the most important predictors of weed suppressive ability. A significant challenge for growers is that cover crop growth can be patchy within fields, making biomass estimation difficult. This study tested ground-based structure-from-motion (SfM) for estimating and mapping cereal rye (*Secale cereale* L.) biomass. SfM generated 3D point clouds from red, green, and blue (RGB) videos collected by a handheld GoPro camera over five fields in North Carolina during the 2022 to 2023 winter season. A model for predicting biomass was generated by relating measured biomass at termination using a density–height index (DH) from point cloud pixel density multiplied by crop height. Overall biomass ranged from 320 to 9,200 kg ha⁻¹, and crop height ranged from 10 to 120 cm. Measured biomass at termination was linearly related to DH ($r^2 = 0.813$) through levels of 9,000 kg ha⁻¹. Based on independent data validation, predicted biomass and measured biomass were linearly related ($r^2 = 0.713$). In the field maps generated by kriging, measured biomass data were autocorrelated at a range of 5.4 to 42.2 m, and predicted biomass data were autocorrelated at a range of 3.4 to 12.0 m. However, the spatial arrangement of high- and low-performing areas was similar for predicted and measured biomass, particularly in fields with greatest patchiness and spatial correlation in biomass values. This study provides proof-of-concept that ground-based SfM can potentially be used to nondestructively estimate and map cover crop biomass production and identify low-performing areas at higher risk for weed pressure and escapes.

Introduction

Cover crops are becoming an increasingly important tool for weed suppression in agriculture (Kumar et al. 2020; Osipitan et al. 2019). The adoption of winter cover crops to diversify weed-suppression tactics and slow the spread of herbicide resistance in weeds is getting global attention (Büchi et al. 2020; Dhanda et al. 2024; Kumar et al. 2020; Osipitan et al. 2019). Cover crops can suppress weeds through multiple mechanisms (Camargo Silva and Bagavathiannan 2023), such as competing directly for resources and/or by physically preventing weed seed germination and seedling growth due to mulch residues left on the soil surface (Baraibar et al. 2018; Dorn et al. 2015; MacLaren et al. 2019; Rueda-Ayala et al. 2015). In addition to the numerous ecosystem services provided by cover crops, such as improved soil moisture, decreased erosion, and increased soil carbon, weed suppression is one of the highest-ranked reasons for adoption by growers (Hamilton 2016; O'Connell et al. 2015).

Cover crop biomass production is one of the most critical factors for determining weed suppression (Baraibar et al. 2018; Campiglia et al. 2012; MacLaren et al. 2019). After termination, the quantity of cover crop residue has been shown to affect weed suppression more than the type of residue (MacLaren et al. 2019; Mirsky et al. 2011). However, biomass production can be extremely variable, both temporally and spatially. This variability can result from factors such as temperature, precipitation, soil type, soil fertility, and topography, or management decisions, including sowing, establishment method, and termination timing (Kumar et al. 2020; Menalled et al. 2022; Mirsky et al. 2011; Muñoz et al. 2014; Nord et al. 2012; Sunoj et al. 2021).

© The Author(s), 2024. Published by Cambridge University Press on behalf of Weed Science Society of America. This is an Open Access article, distributed under the terms of the Creative Commons Attribution licence (<http://creativecommons.org/licenses/by/4.0/>), which permits unrestricted re-use, distribution and reproduction, provided the original article is properly cited.



Cereal rye (*Secale cereale* L.), a widely grown cover crop in the United States due to its winter hardiness, broad climate suitability, and high biomass production potential (Ryan *et al.* 2011), has been shown to suppress weeds up to 100% under ideal conditions in certain regions of the country. Although cereal rye releases phytotoxic compounds that can suppress weeds, the primary driver of weed suppression is the ability to create a thick mulch (Menalled *et al.* 2022; Ryan *et al.* 2011; Smith *et al.* 2011; Teasdale and Mohler 2000). Cereal rye biomass levels directly affect weed suppression and have been shown to decrease weed emergence exponentially with increasing mulch rates (Teasdale and Mohler 2000). However, as with other cover crops, cereal rye growth and biomass production can be highly variable and uneven on a subfield level, resulting in variable degrees of weed suppression (Baraibar *et al.* 2018; Eslami and Davis 2018; Ryan *et al.* 2011; Sunoj *et al.* 2021; Wells *et al.* 2014). This patchiness in cover crop performance poses significant management challenges for growers. Areas of low cover crop performance are more likely to have more late-season weed escapes, which can replenish the soil seedbank and increase future weed problems (Bagavathiannan and Norsworthy 2012; Bagavathiannan *et al.* 2013; Baraibar *et al.* 2018).

To effectively use cover crops for weed suppression, it is essential to have methods for estimating cover crop performance in the field and accordingly identifying areas with high or low risk of in-season weed pressure and potential late-season weed escapes (Bagavathiannan and Norsworthy 2012; Baraibar *et al.* 2018; Sunoj *et al.* 2021; Teasdale and Mohler 2000). Manual sampling, such as mapped grid counts or quadrat harvesting, is laborious and cost-prohibitive and does not adequately characterize the spatial variability of cover crops on a field scale (Sunoj *et al.* 2021; Swoish *et al.* 2022). Satellite- and unmanned aerial vehicle (UAV)-based remote sensing methods using vegetation indices, particularly the normalized difference vegetation index (NDVI), have been shown to predict cover crop biomass reasonably accurately, especially in monoculture grasses (Hively *et al.* 2020; Prabhakara *et al.* 2015). While these techniques have the advantage of being nondestructive, they often lose their sensitivity at canopy closure when the reflectance is saturated and increases in biomass are not detectable (Prabhakara *et al.* 2015; Yue *et al.* 2019).

To address some of these challenges, photogrammetric techniques such as structure-from-motion (SfM) have recently been investigated for estimating cover crop biomass (Roth and Streit 2018; Yue *et al.* 2019). Using photogrammetry, overlapping red, green, and blue (RGB) images can be mosaicked to create digital surface models and 3D point clouds of the crop canopy (Dobbs *et al.* 2022). Previous studies have used UAV-based SfM in conjunction with vegetation indices and canopy height to estimate cover crop biomass (Roth and Streit 2018; Yue *et al.* 2019). However, few studies have attempted to estimate biomass of cover crops using ground-based approaches, which have the advantage of being able to generate extremely detailed canopy models by virtue of being close to the canopy (Deery *et al.* 2020; Dobbs *et al.* 2023; Yue *et al.* 2019; Zhu and Lin 2010). In addition, using ground-based approaches with tractor-mounted cameras takes advantage of the tractor already passing through the field, which is required to terminate the cover crop (Keene *et al.* 2017; Wallace *et al.* 2023).

The present study tested a ground-based SfM technique for estimating cereal rye biomass and mapping biomass distribution on a field scale. The biomass estimation method was developed in a previous study where 3D point clouds were used to estimate biomass at individual sampling points (Dobbs *et al.* 2023). It was

hypothesized that this application of SfM, by virtue of being ground-based, would provide high enough resolution to generate accurate estimates of cover crop biomass on a 2D plane and identify low-performing areas at higher risk for weed infestation and late-season weed escapes.

Materials and Methods

Study Sites

Data were collected between January and April 2023 in five fields, which were located within a 17-ha experimental area (35.396°N, 78.04°W) at the North Carolina Department of Agriculture Cherry Research Farm in Goldsboro, NC, USA. Each field was 10-m wide by 60-m long. Fields were separated by buffer fallow areas (at least 30 m), and some fields had different orientations. The soil in two fields was a Leaf loam (fine, mixed, active, thermic Typic Albaquults), and in the other three fields was a combination of Leaf loam and Pantego loam (fine-loamy, siliceous, semiactive, thermic Umbric Paleaquults). Field location was chosen to ensure variability in cereal rye growth based on historical observations provided by the research farm personnel. The fields were planted using a drill seeder with cereal rye ('Rhymin') as a cover crop in October 2022 at a rate of 68 kg ha⁻¹ with 19-cm row spacing (approximately 48 plants m⁻²) following maize (*Zea mays* L.) in a conventional tillage system, with no residual herbicides applied before planting. The cover crop was terminated in April 2023 with glyphosate at 840 g ae ha⁻¹ (Roundup PowerMax®, Bayer Crop Science, St Louis, MO, USA) and then roller-crimped in the same direction in all five fields. In previous seasons, all of the fields had been planted with soybean [*Glycine max* (L.) Merr.] (also with conventional tillage), with glyphosate and 2,4-D used for weed control.

Video Image Collection

In all five fields, videos were recorded over the cover crop by walking in different 15-m transects each time throughout each field with a GoPro Hero 8 camera (GoPro, San Mateo, CA, USA) attached to a monopod. The camera was held 1.5 m above the ground, facing forward and tilted 45° from horizontal (tilt = -45, roll = 0), creating a 2-m-wide view area. Each video was recorded by walking with a metronome at 60 beats min⁻¹ (approximately 1 m s⁻¹). Two videos were recorded in each transect, one in each direction (to and fro), walking parallel to the cover crop rows. The videos were recorded at this height and speed to mimic a ground-based camera attached to the front of a combine or tractor (Figure 1). This system would record videos at regular intervals over the field to generate 3D point clouds. Within each transect, five red rubber balls (5.5-cm diameter) were placed at 1 m above the soil surface mounted on polyvinyl chloride (PVC) pipes that were spaced 2 m apart to serve as height references and markers for the sampling area for video analysis. All videos were recorded using a 16:9 aspect ratio (3,840 by 2,160 pixels), linear field of view, and 4K resolution at 60 frames s⁻¹, with vertical, horizontal, and diagonal fields of view of 55.2°, 85.8°, and 93.7°, respectively.

In one of the fields, three GoPro videos were recorded every 2 to 3 wk from January until termination (34 videos total) to create a calibration curve for estimating cover crop biomass using image data. Videos were recorded at the tillering (Zadok's stages 21 and 30), elongation (Zadok's stages 31–32 and 39–40), boot (Zadok's stages 41–43), and heading stages (Zadok's stages 50–58). Each video was recorded over a different 15-m transect placed

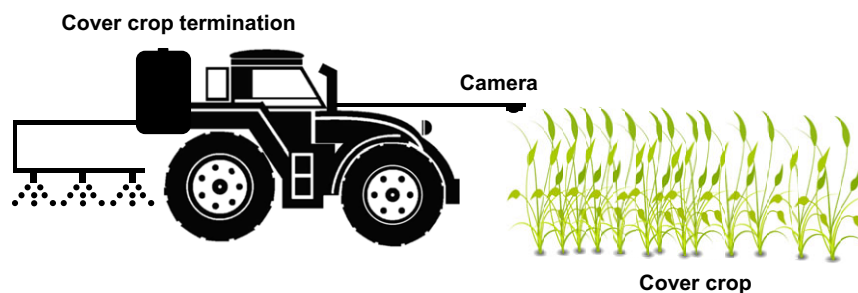


Figure 1. Diagram of the proposed tractor-mounted system, where the camera mounted on the front of the tractor records videos over the cover crop immediately before the crop is terminated.



Figure 2. Still image frame (left) from GoPro videos taken over the cover crop, and 3D point cloud (right) of the same area in the field generated using structure-from-motion.

randomly in the field. In each of the remaining four fields, 32 videos (16 in each direction, to and fro) were recorded 1 wk before termination (heading stage) to test the predictive ability of the model created from the calibration curve (Hildebrandt et al. 2022). In these four fields, the videos were recorded parallel to the long edge of the field, such that each pair of videos covered a different 15-m transect.

Ground Truth Data

Ground truth data were collected within each transect immediately after video recording, sampling five 0.25-m² quadrats spaced 2 m apart. Each quadrat was centered around one of the PVC markers to ensure that all measurements corresponded to known physical locations in the video. Crop height of three randomly selected plants per quadrat was measured and averaged. Crop height was measured from the soil surface to the top of the highest expanded leaf using a meter stick, to the nearest centimeter. Fresh biomass was measured in the field by harvesting all of the cereal rye in each quadrat to ground level. Weeds or other species (a very small proportion of the overall biomass) were not included. Dry biomass was calculated for each quadrat based on the average percent moisture content of a subset consisting of 10 samples dried at 65 C for 72 h. In the field used to create the calibration curve, a total of 102 quadrats were sampled for ground truth data. In the other four fields, 80 quadrats per field were sampled in a 2 m by 2 m grid.

Video Processing

Each video was processed to generate 3D point clouds using an SfM algorithm in Python (Python Software Foundation, Wilmington, DE, USA). First, each 25- to 30-s video was divided into 250 to 300 overlapping frames. Point clouds were then generated from 40 video frames, spaced 5 frames apart. Approximately 15 point clouds were

created from each video, of which the 5 that were selected corresponded to the locations of the PVC markers for analysis (Figure 2). The green pixels representing vegetation were segmented from the soil using hue thresholds of 60° and 180° on the hue, saturation, value color wheel. This hue range was chosen to include all healthy cover crop plants and exclude all other pixels in the image representing soil, PVC, or red balls. The resulting green pixel count for each point cloud was used to create the predictive biomass model (in the case of the first field) and to then test the accuracy of the model on a field scale (in the case of the remaining four fields).

Biomass Prediction Calibration

To create a predictive model for estimating biomass based on data from the first field, a density–height index (DH) (Dobbs et al. 2023) was calculated for each quadrat using the following equation:

$$DH = \text{point cloud pixels} \times \text{average crop height} \quad [1]$$

where point cloud pixels is the total number of green pixels in the point cloud, and average crop height was based on measurements (cm) conducted within the corresponding quadrat. The resulting DH values from the first field ($n = 102$) were compared with their corresponding dry biomass values using linear regression analysis in SigmaPlot (v. 14.0, Systat Software, San Jose, CA, USA). The coefficient of determination (r^2) and Akaike's information criterion were used as indicators of goodness of fit. The best-fit regression model for dry biomass as a function of DH index was determined as:

$$\text{Biomass} = 0.0009 \times DH - 213.74 \quad [2]$$

This equation was used to calculate predicted biomass in the quadrats for the remaining four fields ($n = 320$), where the

predicted biomass for each quadrat was calculated by multiplying the point cloud pixel density by the average crop height. Linear regression was then performed to determine the relationship between predicted and measured biomass across all four fields to determine the predictive ability of the model.

Geostatistics

Predicted and measured biomass values were mapped onto each field in ArcGIS Pro 9.2 (Environmental Systems Research Institute, Redlands, CA, USA). Each pair of values (predicted and measured biomass) was mapped to the measured location of the corresponding sampling quadrat. Ordinary kriging was used to interpolate predicted and measured biomass to a continuous map for each field. Kriging semivariograms were generated for each field separately using 5 neighbors and 12 lags to create an interpolated grid with a cell size of 0.25 m², which was the same as the area of the sampling quadrats. The semivariograms for predicted and measured biomass for each field were derived using the following formula:

$$\gamma(h) = \frac{1}{2m(h)} [\sum (Z_{Xi+h} - Z_{Xi})^2] \quad [3]$$

where γ is the semivariance at lag distance h , $m(h)$ is the number of sample value pairs separated by h , and Z_{Xi} and Z_{Xi+h} represent the sample values at two points Xi and $Xi+h$ locations in the field, respectively (Curran 1988; Verma et al. 2018). This kriging method is commonly used to map vegetation and soil properties and had the lowest root mean-square error (RMSE) of the inverse distance weighting, spline interpolation, and regression kriging methods (Voltz and Webster 1990; Zhu and Lin 2010). Normality, spatial autocorrelation, and stationarity assumptions for data in each field were verified using ArcGIS. All kriging models were evaluated using RMSE and leave-one-out cross-validation, in which a single data point was removed from the dataset and the remaining points were used to predict the value of the point that was removed (Pang et al. 2023). The range (the distance at which data points were no longer spatially autocorrelated), sill (the semivariance at which spatial autocorrelation was no longer present), and nugget (the difference in values at a separation distance of zero, which is a measure of error) was calculated for each semivariogram. Based on these values, the nugget-to-sill ratio was calculated for each semivariogram to quantify the spatial dependence of the data for measured and predicted biomass. A ratio of <25% indicated strong spatial dependence, 25% to 50% indicated moderate spatial dependence, and >75% indicated weak spatial dependence (high unexplained variability) (Rüth and Lennartz 2008; Shit et al. 2016; Venteris et al. 2014).

UAV Imagery

UAV images were collected on the same day as the GoPro video collection before cover crop sampling. Images were collected using a Mavic 3 Multispectral UAV (DJI Technology, Shenzhen, China) flown at 15-m elevation in a grid pattern, with the camera pointing in the nadir direction. Flights were performed within 2 h of solar noon with little to no cloud cover.

Results and Discussion

The measured dry biomass across all five fields in this study ranged from 320 to 9,200 kg ha⁻¹ across all sampling dates. In the field where the calibration measurements were taken throughout the

season, the measured dry biomass range was 420 to 8,000 kg ha⁻¹, with crop height ranging from 10 to 100 cm. The average crop height in the other four fields (referred to as Fields 1 to 4 for the remainder of the discussion) ranged from 35 to 120 cm, although in the majority of sampling points, the crop was 50- to 100-cm tall. The variation in biomass across fields allowed analysis of a broad range of crop biomass levels that could be detected with UAV imagery (Figure 3). However, crop height alone was a poor predictor of biomass, as there was considerable variability in biomass at each crop height. For example, biomass values for quadrats where the average height was approximately 100 cm ranged from 2,000 to 9,000 kg ha⁻¹ (Figure 4).

Due to the significant range in crop height, both throughout the season and at the time of termination, and the fact that the SfM algorithm did not detect lower canopy layers when the crop was taller, integrating height with point cloud pixel density was necessary for producing a more accurate estimation of biomass. In contrast to the regression of crop height and measured biomass (Figure 4), the calibration model comparing DH and biomass showed an approximately 1:1 relationship, with an $r^2 = 0.813$ (Figure 5). Based on the predictive model using DH , the predicted biomass and measured biomass across all data points ($n = 320$) were linearly related with $r^2 = 0.713$ (Figure 6).

As seen in the created field maps for Fields 1 to 4, the high and low areas of measured biomass were in locations similar to the predicted high and low areas (Figure 7). However, there were noticeable differences among fields in the robustness of the kriging model. In Field 1, the semivariograms for measured and predicted biomass showed a similarly clear spatial dependence in the linear portion of the graph throughout a range of 10.8 and 12.0 m, respectively (Figure 8; Table 1). In addition, the difference between predicted and measured biomass in Field 1 was exclusively either zero or negative, indicating that the prediction was either equal to or larger than the measured biomass (Figure 7). Both kriging models also had nugget:sill ratios indicating moderate spatial dependence in the data (Table 1). The accuracy of the biomass predictions for Field 1 appears to be due to greater patchiness and spatial dependence, as well as an overall wider range in biomass values compared with the other four fields. For example, in Fields 2 and 3, the overall variability in measured biomass was considerably lower, and there was much greater discrepancy between the kriging models for measured and predicted biomass (Figure 8). In Field 2, the data for measured biomass showed moderate spatial dependence and leveled off at 42.2 m, while the data for predicted biomass showed weak spatial dependence and leveled off at 3.7 m (Figure 8; Table 1). In Field 3, both measured and predicted biomass showed moderate spatial dependence based on their nugget:sill ratios, with the autocorrelation leveling off at 18.6 m and 5.4 m, respectively (Figure 8; Table 1). Interestingly, in Field 4, which had more variability in measured biomass compared with Fields 2 and 3, there was a similarly robust prediction of biomass, as in Field 1. Field 4 also showed an extremely high level of spatial dependence for both measured and predicted biomass, with a nugget:sill ratio of just 0.1%. In addition, the spatial correlation leveled off at just 5.4 m for both measured and predicted data (Table 1). This is also apparent in the field map for Field 4, which shows clearly similar patterns and sizes of high and low biomass patches for measured and predicted data (Figure 7).

Across all four fields, in areas of higher biomass, the predicted biomass was approximately 1,000 to 1,500 kg ha⁻¹ higher than what was measured and, in a few cases, by as much as 3,140 kg ha⁻¹ (i.e., orange and red in biomass difference maps; Figure 7).

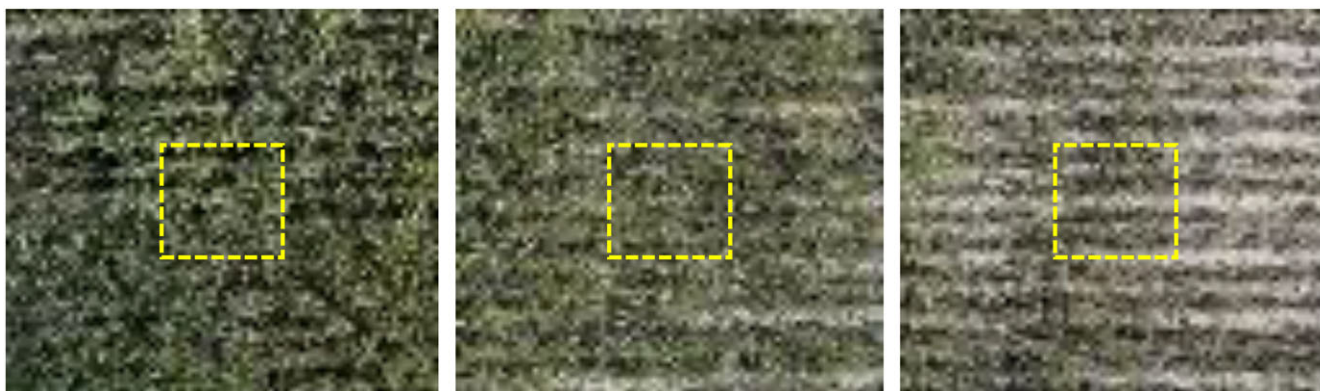


Figure 3. Unmanned aerial vehicle (UAV) images of cereal rye at biomass levels of 7,200 kg ha⁻¹ (left), 5,200 kg ha⁻¹ (center), and 1,200 kg ha⁻¹ (right). The yellow squares indicate 0.25-m² sampling quadrats. All images were acquired at an altitude of 15 m.

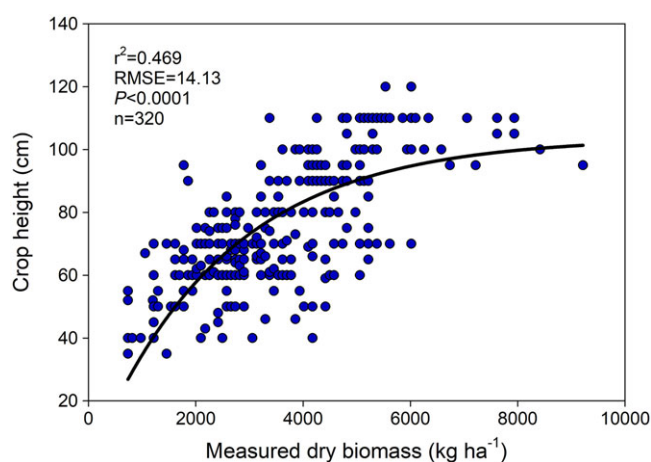


Figure 4. Nonlinear regression of measured dry biomass and crop height. Each point represents one 0.25-m² quadrat. Data are pooled across all four fields ($n = 320$).

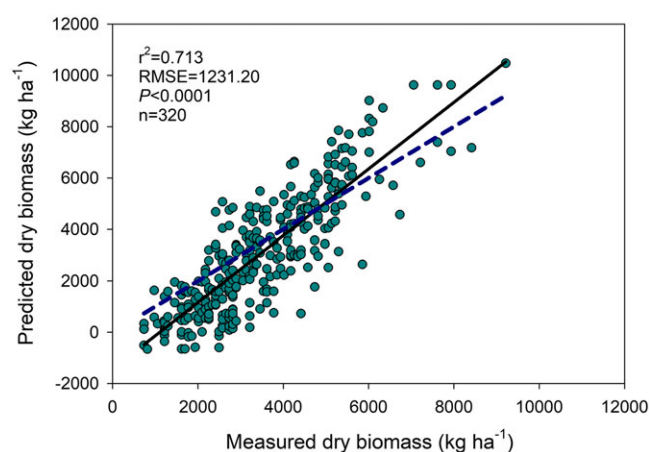


Figure 6. Linear regression of predicted vs. measured cereal rye dry biomass (solid line) from 320 quadrats (circles) pooled across four fields. The dashed line indicates the slope of a theoretical 1:1 relationship between predicted and measured biomass. RMSE, root mean-square error.

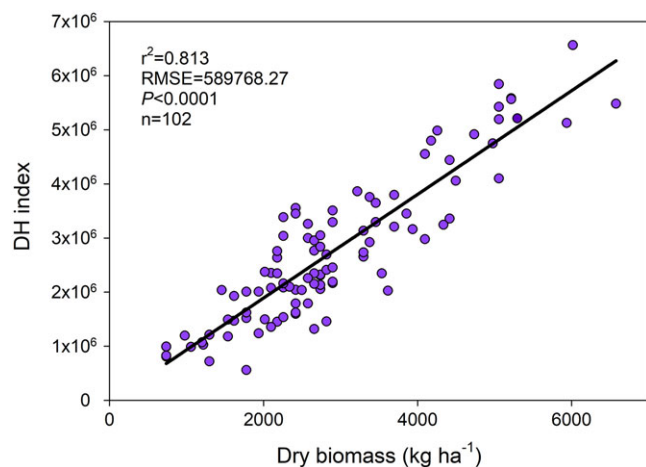


Figure 5. Linear regression of density–height (DH) index and dry biomass from the calibration field. RMSE, root mean-square error.

Conversely, in lower-biomass areas, the model underestimated the biomass at similar levels and, in extreme cases, by as much as 2,837 kg ha⁻¹ (i.e., light and dark green in biomass difference maps; Figure 7). The linear regression between predicted and estimated biomass also reflects this trend, as the slope was steeper than it

would have been at 1:1 (Figure 6). This is partially due to the bias introduced by calculating predicted biomass by multiplying point cloud pixel density by average crop height within each quadrat. In areas of lower biomass, where the crop had sparse cover, the SfM algorithm was less likely to detect all of the individual plants and leaves, especially if there was any excessive movement of the foliage caused by wind or trampling. Therefore, even in areas where the crop was sparse but tall, biomass predictions were lower due to the low pixel density. In higher-biomass areas, the individual plants were approximately 100-cm tall (Figure 4). Even in cases where there was variation in height within a single quadrat, the fact that crop height was averaged across three plants meant that the tallest measurements likely skewed the average for that quadrat. This introduced a bias in high crop height values, which caused overpredictions of biomass by multiplying pixel density by a single uniform height within that quadrat.

Despite the variability in biomass predictions, the present study serves as a proof of concept to identify the potential for and challenges to improving prediction accuracy. Further testing in large commercial farms, over multiple growing seasons, and in multiple locations is warranted. In addition, it is still unknown how crop management variability could modify the relationship between SfM image generation and biomass. Factors such as

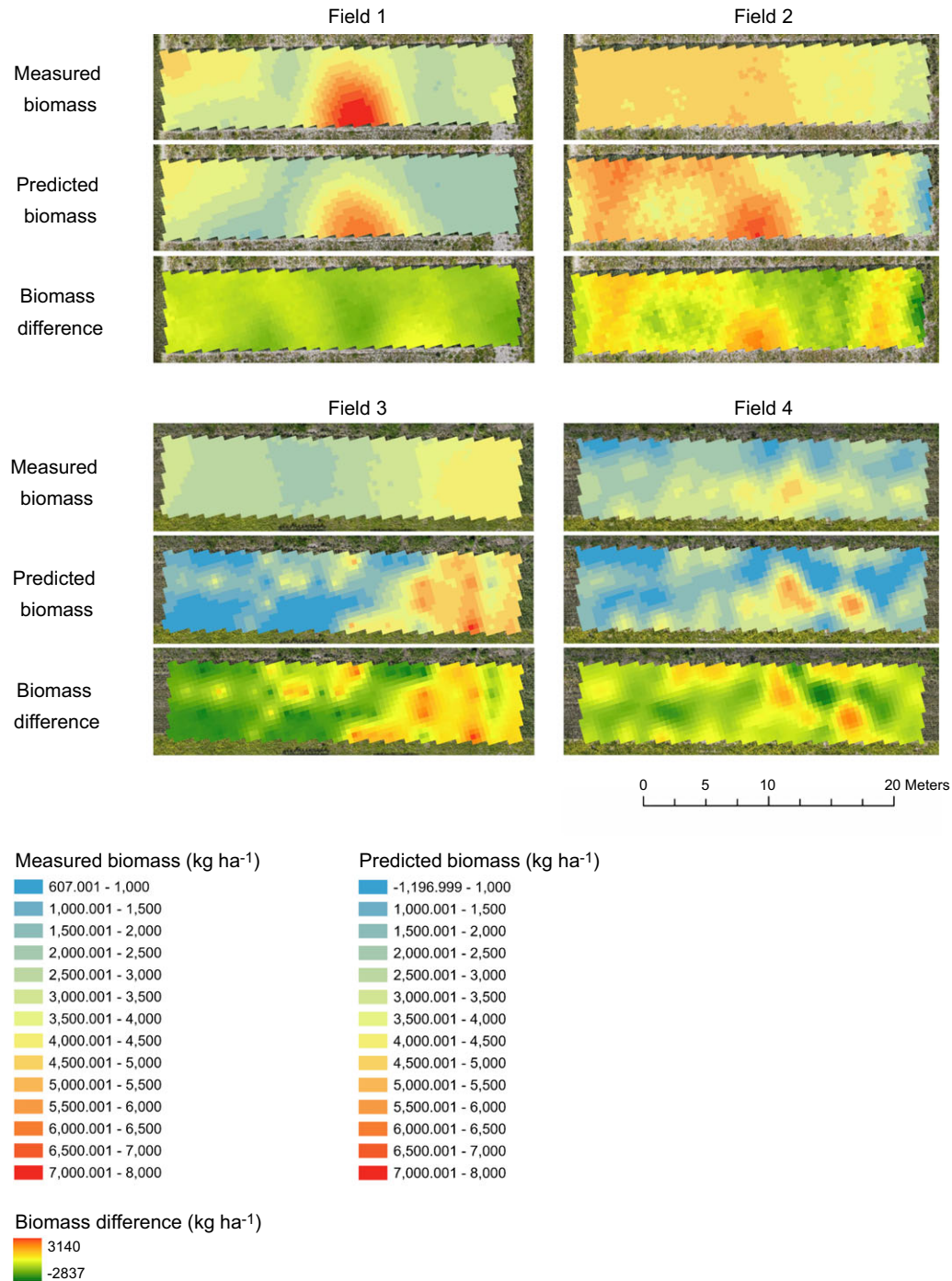


Figure 7. Kriging maps of measured dry biomass, predicted dry biomass, and the difference between predicted and actual biomass, superimposed on unmanned aerial vehicle (UAV) images of four fields.

variation in morphology and growth patterns among varieties of cereal rye as well as differences in planting densities and equipment will certainly affect image collection, processing, and re-creation of canopy structure.

In addition to increased accuracy, there are several significant improvements that would be required for commercial applications of this technology for growers. First, the method in the study did not have a real-time measurement of crop height. While the SfM generated point clouds by triangulating the location of points relative to the camera and soil surface, it did not assign a height

value to the points (Dobbs *et al.* 2022). Therefore, for this method to be more accurate and efficient, crop height would need to be measured automatically, whether by using a depth camera or a sensor or by incorporating height measurements into the SfM algorithm. Second, because the SfM point clouds were generated based on common features in overlapping images, any excessive movement in the canopy due to wind or trampling caused the algorithm to discard those feature points, leading to sparse, less informative point clouds. Third, this method is able to generate point clouds using a simple (and relatively inexpensive) RGB

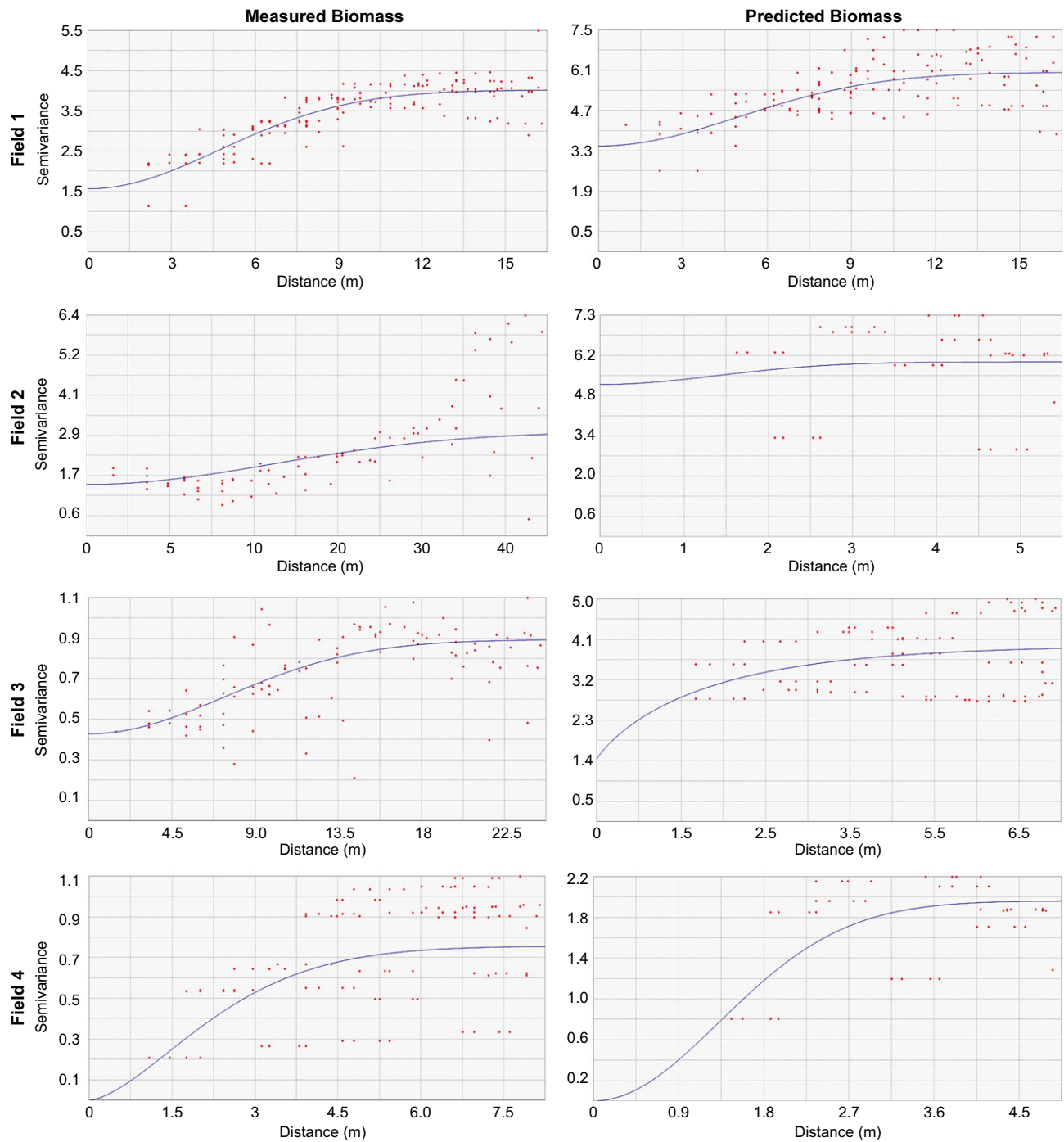


Figure 8. Kriging semivariograms of measured biomass and predicted biomass for Fields 1–4, showing fitted models (solid blue lines) for spatial autocorrelation between pairs of measured sampling points (red dots).

camera, but the algorithm requires extensive computing power. For example, generating clouds for 80 sampling points in a single field in this study required 2 to 3 d of processing using a more powerful computer than most home computers. After taking videos over the field, the grower would upload them to a cloud-based server, generating the point clouds and creating a map of predicted biomass using kriging. Although the present study created biomass maps using sampling in a 2 by 2 m grid, a reasonably accurate map could potentially be generated using fewer samples, which would reduce the computing time.

Therefore, depending on the relative variability of biomass in the field, the sampling frequency could be optimized and generate a reasonably accurate map of biomass using the shortest possible computing time. The grower could visually estimate the level of evenness of biomass (e.g., on a scale of 1 to 10), which would automatically adjust the sampling rate of videos.

Based on this proof-of-concept study, this ground-based approach using SfM has the potential for estimating biomass in cover crops on a field scale. With improved accuracy, it could help growers not only to monitor cover crops, but also to predict and

Table 1. Summary of statistics for kriging models for Fields 1–4

Field	Parameter	Semivariance		Nugget:sill	Range	RMSE ^a
		Nugget	Sill			
		kg ha ⁻¹		%	m	
1	Measured biomass	1,584,452	4,075,329	38.9	10.8	1,488.8
1	Predicted biomass	3,558,163	6,050,401	58.8	12.0	2,081.7
2	Measured biomass	1,483,569	3,018,791	49.1	42.2	1,365.0
2	Predicted biomass	5,188,991	5,958,774	87.1	3.7	2,564.7
3	Measured biomass	750,391	1,562,740	48.0	18.6	974.7
3	Predicted biomass	1,395,385	3,961,062	35.2	5.4	1,826.0
4	Measured biomass	744	886,311	0.1	5.4	553.2
4	Predicted biomass	2,008	2,009,962	0.1	3.4	1,022.3

^aRMSE, root mean-square error.

manage weed occurrence, including late-season weed escapes. For example, it could be used to identify areas where predicted dry biomass is near or above the level of 7,000 to 8,000 kg ha⁻¹, which is recommended for optimal weed suppression in the subsequent cash crop (Liebert et al. 2017; Teasdale and Mohler 2000). It could also identify areas with low biomass (<2,000 kg ha⁻¹), which are associated with high degrees of weed infestation and late-season weed biomass (Teasdale and Mohler 2000). With additional testing and improvements, this method could potentially be developed into an integrated system for growers to map biomass at the same time as cover crop termination using a tractor-mounted camera or smartphone and identify low-performing areas as being at higher risk for weed pressure (Figure 1). If used at the same time as termination, this would eliminate the need for additional passes through the field. Furthermore, if used before termination, it could inform decisions about expected yield and timing of termination. For example, if the cover crop performance was extremely variable, with lots of low-density patches that could become weedy in the future, this could warrant earlier termination. Finally, due to the relatively inexpensive equipment requirement and potential for automation, this method could be developed and incorporated into existing management systems, presumably in a cost-effective manner.

Acknowledgments. The authors thank Paula Ramos-Giraldo for creating the SfM algorithm Python scripts. In addition, the authors thank Rob Austin (North Carolina State University) for assistance with ArcGIS Pro and the staff at Cherry Research Farm for their help with cover crop management.

Funding statement. This research was supported by the U.S. Department of Agriculture–National Resources Conservation Service Conservation Innovation Grant NR213A750013G031 and the U.S. Department of Agriculture Area-Wide Funds and Hatch Project NC02906.

Competing interests. The authors declare no competing interests.

References

- Bagavathiannan MV, Norsworthy JK (2012) Late-season seed production in arable weed communities: management implications. *Weed Sci* 60:325–334
- Bagavathiannan MV, Norsworthy JK, Smith KL, Neve P (2013) Modeling the evolution of glyphosate resistance in barnyardgrass (*Echinochloa crus-galli*) in cotton-based production systems of the midsouthern United States. *Weed Technol* 27:475–487
- Baraibar B, Hunter MC, Schipanski ME, Hamilton A, Mortensen DA (2018) Weed suppression in cover crop monocultures and mixtures. *Weed Sci* 66:121–133
- Büchi L, Wendling M, Amossé C, Jeangros B, Charles R (2020) Cover crops to secure weed control strategies in a maize crop with reduced tillage. *Field Crops Res* 247:107583
- Camargo Silva G, Bagavathiannan M (2023) Mechanisms of weed suppression by cereal rye cover crop: a review. *Agron J* 115:1571–1585
- Campiglia E, Radicetti E, Mancinelli R (2012) Weed control strategies and yield response in a pepper crop (*Capsicum annuum* L.) mulched with hairy vetch (*Vicia villosa* Roth.) and oat (*Avena sativa* L.) residues. *Crop Prot* 33:65–73
- Curran PJ (1988) The semivariogram in remote sensing: an introduction. *Remote Sens Environ* 24:493–507
- Deery DM, Rebetzke GJ, Jimenez-Berni JA, Condon AG, Smith DJ, Bechaz KM, Bovill WD (2020) Ground-based LiDAR improves phenotypic repeatability of above-ground biomass and crop growth rate in wheat. *Plant Phenomics* 2020:8329798
- Dhanda S, Kumar V, Dille JA, Obour A, Yeager EA, Holman J (2024) Influence of cover crop residue and residual herbicide on emergence dynamics of glyphosate-resistant Palmer amaranth (*Amaranthus palmeri*) in grain sorghum. *Weed Sci* 72, 10.1017/wsc.2024.22
- Dobbs AM, Ginn D, Skovsen SK, Yadav R, Jha P, Bagavathiannan MV, Mirsky SB, Reberg-Horton CS, Leon RG (2022) New directions in weed management and research using 3D imaging. *Weed Sci* 70:641–647
- Dobbs AM, Ginn D, Skovsen SK, Yadav R, Jha P, Bagavathiannan MV, Mirsky SB, Reberg-Horton CS, Leon RG (2023) Using structure-from-motion to estimate cover crop biomass and characterize canopy structure. *Field Crops Res* 302:109099
- Dorn B, Jossi W, van der Heijden MGA (2015) Weed suppression by cover crops: comparative on-farm experiments under integrated and organic conservation tillage. *Weed Res* 55:586–597
- Eslami SV, Davis AS (2018) Weed interference with no-till soybeans influenced by fine-scale covariation between soil properties and cover crop performance. *Weed Res* 58:463–474
- Hamilton A (2016) Maximizing the On-Farm Benefits of Cover Crops: Comparing Management Intentions and Ecosystem Service Provisioning. Master's thesis. University Park: Pennsylvania State University. 227 p
- Hildebrandt C, Haley S, Shelton CW, Westra EP, Westra P, Gaines T (2022) Winter annual grass control and crop safety in quizalofop-resistant wheat cultivars. *Agron J* 114:1374–1384
- Hively WD, Lee S, Sadeghi AM, McCarty GW, Lamb BT, Soroka A, Keppler J, Yeo I-Y, Moglen GE (2020) Estimating the effect of winter cover crops on nitrogen leaching using cost-share enrollment data, satellite remote sensing, and Soil and Water Assessment Tool (SWAT) modeling. *J Soil Water Conserv* 75:362–375
- Keene CL, Curran WS, Wallace JM, Ryan MR, Mirsky SB, VanGessel MJ, Barbercheck ME (2017) Cover crop termination timing is critical in organic rotational no-till systems. *Agron J* 109:272–282
- Kumar V, Obour A., Jha P, Liu R, Manuchehri MR, Dille JA, Holman J, Stahlman PW (2020) Integrating cover crops for weed management in the semiarid US Great Plains: opportunities and challenges. *Weed Sci* 68:311–323
- Liebert JA, DiTommaso A, Ryan MR (2017) Rolled mixtures of barley and cereal rye for weed suppression in cover crop–based organic no-till planted soybean. *Weed Sci* 65:426–439
- MacLaren C, Swanepoel P, Bennett J, Wright J, Dehnen-Schmutz K (2019) Cover crop biomass production is more important than diversity for weed suppression. *Crop Sci* 59:733–748

- Menalled UD, Adeux G, Cordeau S, Smith RG, Mirsky SB, Ryan MR (2022) Cereal rye mulch biomass and crop density affect weed suppression and community assembly in no-till planted soybean. *Ecosphere* 13:e4147
- Mirsky SB, Curran WS, Mortensen DM, Ryany MR, Shumway DL (2011) Timing of cover-crop management effects on weed suppression in no-till planted soybean using a roller-crimper. *Weed Sci* 59:380–389
- Muñoz JD, Steibel JP, Snapp S, Kravchenko AN (2014) Cover crop effect on corn growth and yield as influenced by topography. *Agric Ecosyst Environ* 189:229–239
- Nord EA, Ryan MR, Curran WS, Mortensen DA, Mirsky SB (2012) Effects of management type and timing on weed suppression in soybean no-till planted into rolled-crimped cereal rye. *Weed Sci* 60:624–633
- O'Connell S, Grossman JM, Hoyt GD, Shi W, Bowen S, Marticorena DC, Fager KL, Creamer NG (2015) A survey of cover crop practices and perceptions of sustainable farmers in North Carolina and the surrounding region. *Renew Agric Food Syst* 30:550–562
- Osipitan OA, Dille JA, Assefa Y, Radicetti E, Ayeni A, Knezevic SZ (2019) Impact of cover crop management on level of weed suppression: a meta-analysis. *Crop Sci* 59:833–842
- Pang Y, Wang Y, Lai X, Zhang S, Liang P, Song X (2023) Enhanced kriging leave-one-out cross-validation in improving model estimation and optimization. *Comput Methods Appl Mech Eng* 414:116194
- Prabhakara K, Hively WD, McCarty GW (2015) Evaluating the relationship between biomass, percent groundcover and remote sensing indices across six winter cover crop fields in Maryland, United States. *Int J Appl Earth Obs Geoinf* 39:88–102
- Roth L, Streit B (2018) Predicting cover crop biomass by lightweight UAS-based RGB and NIR photography: an applied photogrammetric approach. *Precis Agric* 19:93–114
- Rueda-Ayala V, Jaeck O, Gerhards R (2015) Investigation of biochemical and competitive effects of cover crops on crops and weeds. *Crop Prot* 71:79–87
- Rüth B, Lennartz B (2008) Spatial variability of soil properties and rice yield along two catenas in southeast China. *Pedosphere* 18:409–420
- Ryan MR, Mirsky SB, Mortensen DA, Teasdale JR, Curran WS (2011) Potential synergistic effects of cereal rye biomass and soybean planting density on weed suppression. *Weed Sci* 59:238–246
- Shit PK, Bhunia GS, Maiti R (2016) Spatial analysis of soil properties using GIS based geostatistics models. *Model Earth Syst Environ* 2:107
- Smith AN, Reberg-Horton SC, Place GT, Meijer AD, Arellano C, Mueller JP (2011) Rolled rye mulch for weed suppression in organic no-tillage soybeans. *Weed Sci* 59:224–231
- Sunoj S, McRoberts KC, Benson M, Ketterings QM (2021) Digital image analysis estimates of biomass, carbon, and nitrogen uptake of winter cereal cover crops. *Comput Electron Agric* 184:106093
- Swoish M, Da Cunha Leme Filho JF, Reiter MS, Campbell JB, Thomason WE (2022) Comparing satellites and vegetation indices for cover crop biomass estimation. *Comput Electron Agric* 196:106900
- Teasdale JR, Mohler CL (2000) The quantitative relationship between weed emergence and the physical properties of mulches. *Weed Sci* 48:385–392
- Venteris ER, Basta NT, Bigham JM, Rea R (2014) Modeling spatial patterns in soil arsenic to estimate natural baseline concentrations. *J Environ Qual* 43:936–946
- Verma RR, Manjunath BL, Singh NP, Kumar A, Asolkar T, Chavan V, Srivastava TK, Singh P (2018) Soil mapping and delineation of management zones in the Western Ghats of coastal India. *Land Degrad Dev* 29:4313–4322
- Voltz M, Webster R (1990) A comparison of kriging, cubic splines and classification for predicting soil properties from sample information. *J Soil Sci* 41:473–490
- Wallace JM, Mazzone T, Larson Z (2023) Cereal rye residue management tactics influence interrow and intrarow weed recruitment dynamics in field corn when planting green. *Weed Technol* 37:422–430
- Wells MS, Reberg-Horton SC, Mirsky SB (2014) Cultural strategies for managing weeds and soil moisture in cover crop based no-till soybean production. *Weed Sci* 62:501–511
- Yue J, Yang G, Tian Q, Feng H, Xu K, Zhou C (2019) Estimate of winter-wheat above-ground biomass based on UAV ultrahigh-ground-resolution image textures and vegetation indices. *ISPRS J Photogramm Remote Sens* 150:226–244
- Zhu Q, Lin HS (2010) Comparing ordinary kriging and regression kriging for soil properties in contrasting landscapes. *Pedosphere* 20:594–606